

Radio halos in nearby ($z < 0.4$) clusters of galaxies

G. Giovannini^{1,2}, A. Bonafede^{1,2}, L. Feretti², F. Govoni³, M. Murgia^{2,3}, F. Ferrari², G. Monti²

(1) Dipartimento di Astronomia, via Ranzani 1, 40127 Bologna, I

(2) Istituto di Radioastronomia-INAf, via P.Gobetti 101, 40129 Bologna, I

(3) Osservatorio Astronomico di Cagliari - INAF, Strada 54, Loc. Poggio dei Pini, 09012 Capoterra (Ca), I

Preprint online version: December 11, 2017

ABSTRACT

Context. The Intra-Cluster Medium is characterized by thermal emission, and by the presence of large scale magnetic fields. In some clusters of galaxies a diffuse non-thermal emission is also present, located at the cluster center and named radio halo. These sources indicate the existence of relativistic particles and magnetic fields in the cluster volume.

Aims. In this paper we collect data on all known nearby cluster radio halos ($z < 0.4$), to discuss their statistical properties and to investigate their origin.

Methods. We searched for published data on radio halos and reduced new and archive VLA data to increase the number of known radio halos.

Results. We present data on 31 radio halos, 1 new relic source, and 1 giant filament. We note the discovery of a small size diffuse radio emission in a cluster (A1213) with very low X-ray luminosity. Among statistical results we confirm the correlation between the average halo radio spectral index and the cluster temperature. We also discuss the high percentage of clusters where both a relic and a radio halo is present.

Conclusions. The sample of radio halos discussed here represents the population of radio halos observable with present radio telescopes. The new telescope generation is necessary for a more detailed multifrequency study, and to investigate the possible existence of a population of radio halos with different properties.

Key words. galaxies:cluster:non-thermal

1. Introduction

The baryonic content of galaxy clusters is dominated by the hot ($T \sim 2 - 10$ keV) intergalactic gas whose thermal emission is observed in X-rays. Thermal emission is a common property of all clusters of galaxies and has been detected even in poor galaxy groups as well as in optical filaments connecting rich clusters.

The Intra-Cluster Medium (ICM) is also characterized by the presence of large scale magnetic fields. A magnetized plasma between an observer and a radio source changes the observed properties of the polarized emission from the radio source. Therefore information on clusters magnetic fields can be determined, in conjunction with X-ray observations of the hot gas, through the analysis of the Rotation Measure (RM) of radio galaxies in the background or in the galaxy clusters themselves. Detailed RM studies have shown that in the ICM large scale magnetic fields at microgauss level (higher in central cooling cluster regions) are present (e.g. Govoni & Feretti 2004, Bonafede et al. 2009b).

In some clusters of galaxies a diffuse non-thermal emission is also present (e.g. Feretti 2005a, Ferrari et al. 2008). These sources indicate the existence of relativistic particles and magnetic fields in the cluster volume, thus the presence of non-thermal processes in the hot ICM.

These large synchrotron sources, which are not obviously associated with any individual galaxy, have been identified as relics, mini-halos, and halos. They are diffuse, low-surface brightness ($\approx 10^{-6}$ Jy/arcsec² at 1.4 GHz), steep-spectrum¹ ($\alpha > 1$) sources, and represent the best evidence for the presence of large-scale magnetic fields and relativistic particles in

the cluster peripheral regions (relics, Giovannini & Feretti 2004, Bonafede et al. 2009a), in the central regions of relaxed clusters (mini-halos, Govoni et al. 2009), and in non relaxed clusters (halos, Feretti 2004). In this paper we will focus on radio halos. A similar review on radio relics is in progress, and we refer to recent papers as Govoni et al. 2009 and Murgia et al. 2009 about mini-halos.

Radio halos are faint, steep-spectrum sources located at the cluster center (e.g. Feretti & Giovannini 2008). Their radio emission is typically unpolarized with the exception of A2255 (Govoni et al. 2005), and MACSJ0717.7+3745 (Bonafede et al. 2009b). Radio halos are typically found in clusters which show significant evidence of an ongoing merger (e.g. Buote 2001, Govoni et al. 2004). It has been proposed that recent cluster mergers may play an important role in the re-acceleration of the radio-emitting relativistic particles, thus providing the energy to these extended sources (e.g. Brunetti et al. 2001, Petrosian 2001).

About 20 radio halos are known from literature data up to now (e.g. Feretti & Giovannini 1998, Feretti 2000, Govoni et al. 2001a, Bacchi et al. 2003, Venturi et al. 2007, Venturi et al. 2008, and Venturi et al. 2009), and their properties have been discussed in different papers. The knowledge of the properties of these sources has increased significantly in recent years, due to higher sensitivity radio images and to the development of theoretical models. The importance of these sources is that they are large scale features, which are related to other cluster properties in the optical and X-ray domain, and are thus directly connected to the cluster history and evolution.

¹ $S(\nu) \propto \nu^{-\alpha}$

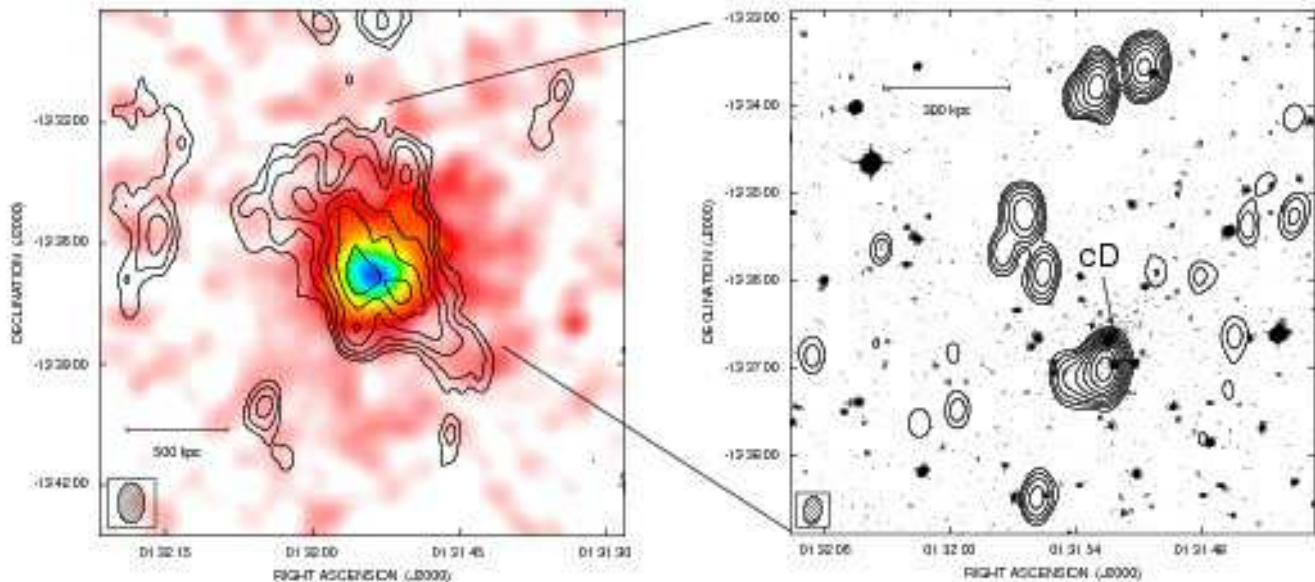


Fig. 1. Left: radio contours of the extended halo in A209 obtained with the VLA at 1.4 GHz combining data in C and D configuration, after subtraction of discrete sources. The HPBW is $60'' \times 40''$ (PA 0°), and the noise level is 0.05 mJy/beam. The first contour level is drawn at 0.2 mJy/beam and the others are spaced by a factor $\sqrt{2}$. We note on the East of the radio halo a faint diffuse emission in N-S direction. The shape and extension suggest its identification with a possible relic source, however because of the low brightness and of the presence of optical candidates further observations are necessary to confirm this. The contours of the radio intensity are overlaid onto the Rosat HRI X-ray image in the 0.1-2.4 keV band. The X-ray image has been smoothed with a Gaussian of $\sigma = 16''$. Right: radio contours obtained with the VLA at 1.4 GHz in C configuration of A209. The HPBW of the radio image is $20.1'' \times 12.8''$ (PA -3°), and the noise level is 0.03 mJy/beam. The first contour level is drawn at 0.07 mJy/beam and the others are spaced by a factor 2. The contours of the radio intensity are overlaid onto the optical red image obtained from the SERC/ESO surveys. The central cD galaxy (pointed out by a line) is marginally visible on the top of the head-tail radio galaxy. Only discrete sources are visible because of the missing of short baselines. Here and in the following figures the restoring HPBW is shown in the bottom left corner.

Here we will present new data and images of radio halos and collect all data published on halos for a statistical study. The organization of this paper is as follows: in Sect. 2 we present new data on nearby ($z < 0.4$) radio halos (a study of the extended emission in rich clusters at redshift > 0.4 is in progress, see e.g. Bonafede et al. 2009b); in Sect. 3 we present new radio halos and report in Table 2 relevant data on all radio halos in nearby clusters known up to date. Correlations and statistical results are discussed in Sect. 4 and Conclusions are reported in Sect. 5.

The intrinsic parameters quoted in this paper are computed for a Λ CDM cosmology with $H_0 = 71 \text{ km s}^{-1} \text{ Mpc}^{-1}$, $\Omega_m = 0.27$, and $\Omega_\Lambda = 0.73$.

2. Observations and data reduction

Here we present new data for radio halos obtained with the VLA at 1.4 GHz. The list of the clusters, together with the observation position, the on source time, the VLA configuration, and the observing date is reported in Tab. 1. Information on final images (angular resolution and noise level) are reported in the figure captions. All new data are from pointed observations, and include proprietary data as well as VLA public archive data.

To derive final images we calibrated the data with the standard technique using the AIPS package. Calibrated data were carefully edited and self-calibrated in phase and gain. To obtain images and flux densities of the extended halo sources, unrelated discrete sources have been subtracted in the uv-plane.

To this aim we produced high resolution images with a uniform weight (ROBUST = -5), and without the short baselines. In these images all discrete sources are present, but the extended diffuse sources (halos or relics) are absent because of the missing of short spacings in the u-v plane.

We checked that the total flux density in the clean components is in agreement with the total flux density visible in the u-v plane. We then selected the clean components of sources to be subtracted (usually in the central region) using the task CCEDT and the AIPS procedure BOX2CC. After a comparison among source flux densities in clean components and from a gaussian fit (task JMFIT), clean components were subtracted from the u-v data. With the new data set we produced images with uniform and natural weights and carefully compared the total flux density present in the short baselines with the total flux in the clean components. Finally we derived the parameters of the diffuse sources.

The error of the flux density of diffuse radio sources has been obtained as due to the combination of the noise level (derived from the individual images), and the uncertainty due to the flux density calibration (estimated of the order of 3%). In addition, in dealing with extended sources, one has to take into account the presence of possible variations in the zero-level of the image. We estimated the zero-level in the images in region free of sources around the radio halos using the AIPS task 'IMEAN', and found that it is very good, and does not affect the measured halo flux density. Finally, the accuracy of the flux density estimate is related to the subtraction of discrete sources. We estimated this

Table 1. Observing parameters

Cluster	RA J2000	DEC J2000	Obs. Time minutes	Array	Date dd-mm-yy
A209	01 31 57.00	-13 34 35.0	20	C	15-APR-2004
			90	D	03-JUL-2004
A521	04 54 12.00	-10 15 00.0	360	B/C	22-SEP-2002
A697	08 42 57.76	+36 21 45.3	50	C	30-MAR-1996
A851	09 42 48.60	+47 00 00.0	20	C	15-MAR-1995
			70	D	03-APR-2000
A1213	11 16 40.00	+29 16 00.0	90	C	06-MAR-2008
			90	C/D	02-JUN-2008
A1351	11 42 32.50	+58 32 08.0	15	D	15-MAR-1995
			120	C	03-APR-2000
A1758	13 32 32.00	+50 30 36.0	150	D	11-MAR-2003
			150	C	06-MAY-2004
A1995	14 52 47.50	+58 03 08.0	120	C	03-APR-2000
			15	D	15-MAR-1995
A2034	15 10 17.00	+33 31 00.0	30	C	06-AUG-2001
			30	D	24-MAR-2003
A2294	17 23 13.80	+85 53 21.0	15	D	15-MAR-1995
			60	C	01-APR-2000
A3444	10 23 50.11	-27 15 15.8	240	A/B	02-OCT-2003
			240	C/D	29-MAY-2004
CL1446+26	14 49 28.70	+26 07 54.10	120	C	01-APR-2000

Col. 1: Cluster Name; Col. 2, Col. 3: Observation pointing (RA J2000, DEC J2000);
Col. 4: On source observing time; Col. 5: VLA configuration; Col. 6: Observing dates.

last point comparing the flux density in clean components subtracted in u-v data with the flux density estimated with a gaussian fit. Final flux density uncertainties are reported in Table 2. For published halos we report the published flux density uncertainty when available. If not published we estimated it as discussed before.

3. New radio halos at 1.4 GHz

We present here new images of radio halos in 10 different clusters (see Tab. 1). Moreover we present new data on two radio halo candidates, which in the light of new data we classify as a giant filament (Abell 3444) and a new relic source (CL1446+26). We found that in A697 (Venturi et al. 2008) and A521 (Brunetti et al. 2008) the diffuse emission previously found only at lower frequency is also clearly visible at 1.4 GHz (see also Dallacasa et al. 2009). Moreover we present improved images at 1.4 GHz for A209, and A1758 previously discussed at this frequency only in conference proceedings. For the other clusters we confirm with pointed observations the presence of a diffuse radio emission. Details on the individual sources are given below.

Abell 209 is a rich cluster of galaxies at $z = 0.206$. It is dominated by a central cD galaxy, and the peak of the cluster mass distribution is close to this galaxy. A candidate gravitational arc is visible inside the cD halo (Dahle et al. 2002). ROSAT HRI data for this cluster indicate an irregular X-ray morphology with significant substructure (Rizza et al. 1998). X-ray data and optical density distribution suggest the presence of a cluster merger (Mercurio et al. 2003). The projected mass distribution estimated with the weak lensing technique (Paulin-Henriksson et al. 2007), shows a pronounced asymmetry, with an elongated structure extending from the SE to the NW. A similar elongation was previously detected in the X-ray

emission map by Rizza et al. 1998, and it is confirmed by the distribution of galaxy colours (Paulin-Henriksson et al. 2007).

In the radio band an extended halo is detected. An image at 1.4 GHz was first presented in Giovannini et al. 2006. Venturi et al. 2007 presented a radio image at 610 MHz obtained with the GMRT but the smaller angular size and low flux density with respect to the 1.4 GHz data, suggest some missing flux in GMRT data.

In Fig. 1 we show the central cluster radio emission compared with optical and X-ray images. On the left we present the radio contours of the extended halo source obtained by combining C and D configuration data. Discrete radio sources have been subtracted as discussed before. The halo total flux density is 16.9 mJy and the largest size is $\sim 7'$ in PA $\sim 45^\circ$. On the East of the radio halo an extended elongated structure is present at about 4σ level, possibly identified as a peripheral relic radio source. A deeper VLA image is necessary to confirm the detection and to study it in more detail. For a comparison between the radio and the X-ray cluster emission, the contours of the radio intensity are overlaid onto the Rosat HRI X-ray image in the 0.1-2.4 keV band. On the right we present a zoom of a full resolution image obtained with the VLA in the C-array of the cluster center overlaid onto an optical image. The optical images herein were taken from the Optical Digitized Sky Survey². Because of the angular resolution and the missing of short baselines only discrete sources are visible. The central cD galaxy appears to be radio quiet, but a head-tail radio galaxy is visible near the cluster center.

Abell 521 at $z = 0.2533$ has been studied in detail in the optical and X-ray using Chandra observations (Ferrari et al. 2006). A521 is a spectacular example of a multiple merger cluster made up of several substructures converging at different epochs towards the centre of the system. The very perturbed dynamical state of this cluster is also confirmed by the discovery of a ra-

² See <http://archive.eso.org/dss/dss>

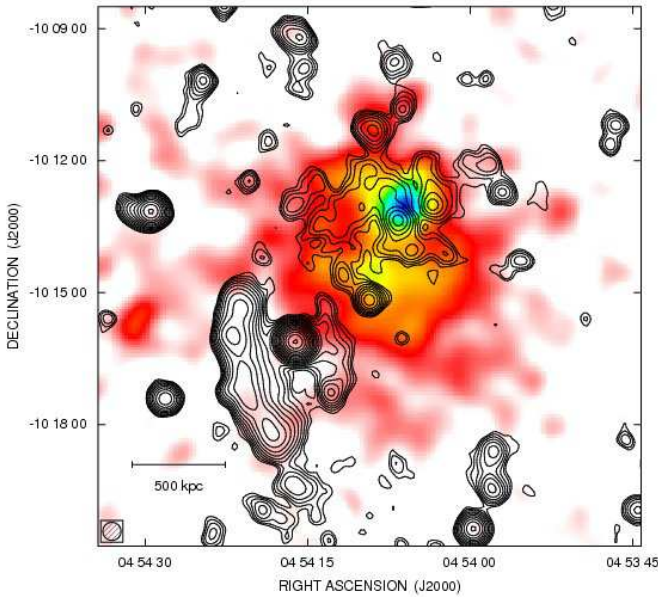


Fig. 2. Radio contours of the complex region in A521 obtained with the VLA at 1.4 GHz in B/C configuration. The HPBW is $25'' \times 25''$ and the noise level is 0.03 mJy/beam. The central diffuse halo source is well visible as well as the extended relic (see text). The first contour level is drawn at 0.06 mJy/beam and the others are spaced by a factor $\sqrt{2}$. The contours of the radio intensity are overlaid onto the Rosat HRI X-ray image in the 0.1-2.4 keV band. The X-ray image has been smoothed with a Gaussian of $\sigma = 16''$.

radio relic in its South-East region, using VLA observations in the B/C configuration at 1.4 GHz (Ferrari et al. 2006). This relic source has been studied also at lower frequency with GMRT data (Giacintucci et al. 2006, Giacintucci et al. 2008).

Brunetti et al. 2008 reported the detection of a diffuse halo at the cluster center visible in GMRT data at 240, 325, and 610 MHz. They also reported a flux density upper limit at 74 MHz from the VLA Low-frequency Sky Survey data and discussed the missing detection at 1.4 GHz from VLA archive data. They found that this halo has an extremely steep radio spectrum (~ 2.1) with a high frequency cut-off.

We independently reanalyzed the VLA archive data to search for a possible diffuse radio halo. After carefully editing of the uv data we produced an image cutting the long baselines, and giving a large weight to short baselines using ROBUST = 5 in the AIPS task IMAGR (Natural weight). The image obtained clearly shows an extended emission not visible in previous images because of its low brightness. In Fig. 2 we present the radio contours of this low resolution image overlaid onto the Rosat HRI X-ray image in the 0.1-2.4 keV band. The radio halo is well visible, and also the relic source appears more diffuse than in previous images. Moreover a new extended emission almost parallel to the relic but less extended is visible. The radio halo morphology in the present image is in good agreement with lower frequency images reported by Brunetti et al. 2008, although their image at 240 MHz shows a larger extension because of a better uv-coverage and a larger beam, and with a more recent VLA image by Dallacasa et al. 2009.

We subtracted the contribution of discrete sources as discussed in Sect. 2. The flux density emission from the diffuse source was $S_{tot} = 7.0$ mJy, in the original image including dis-

crete sources. After subtraction of discrete sources (1.1 mJy in total), the halo flux density is 5.9 mJy.

We compared our flux density measure with the values reported by Brunetti et al. 2008: ($S_{240} = 152$ mJy, $S_{325} = 90$ mJy, $S_{610} = 15$ mJy), and derived a straight radio spectrum between 240, 325 and 1415 MHz with a constant spectral index $\alpha = 1.8$. We note that the value at 610 MHz is lower than that implied by a straight spectrum, probably because of missing flux in GMRT data at this frequency.

Abell 697, a massive cluster at $z = 0.282$, shows a central cD galaxy with a peculiar disturbed morphology, indicative of a recent merger. The mass distribution is elongated in NE - SW direction. The central cD galaxy has a double nucleus, which also supports the merger hypothesis. An X-ray ROSAT HRI observation shows an elliptical X-ray luminosity distribution in N-S direction (see also Girardi et al. 2006).

In the radio band an extended halo was detected by Venturi et al. 2008 using GMRT data at 610 MHz and recently at 325 MHz (Venturi et al. 2009). The halo flux density at 325 MHz is 45 mJy and 13 mJy at 610 MHz, resulting in a very steep radio spectrum ($\alpha_{0.3}^{0.6} \sim 2$, Venturi et al. 2009). Here we present a new image obtained using archive VLA data at 1415 MHz in the C configuration. In Fig. 3 we present the radio contours of this image overlaid onto the Rosat HRI X-ray image in the 0.1-2.4 keV band. The image confirms the presence of central diffuse emission. The total flux density is 1.7 mJy, and the noise level is 0.1 mJy/beam. A comparison between present data, and the NVSS, and Venturi et al. 2008 shows that in the C array VLA data most of the extended flux is missing (indeed the NVSS flux density is 7.8 mJy). Therefore we report in Tab. 2 the 1.4 GHz flux density and size estimated from the NVSS. Comparing NVSS and GMRT data at 325 MHz we derive a halo spectral index $\alpha_{0.3}^{1.4} \sim 1.2$. A deeper VLA image at 1.4 GHz is necessary to confirm this result.

Abell 851 - CL0939+4713 is a rich cluster of galaxies at $z = 0.4069$. A study by Sato & Martin 2006 shows a high number of starburst galaxies probably due to some cluster-specific mechanism, likely related to the dynamical assembly of the cluster. The existence of an extended diffuse emission in this cluster was first reported by Owen et al. 1999. We reduced C, and D archive VLA data at 1400 MHz. In Fig. 4 we present the radio contours of A851 overlaid onto the optical image from the POSS2 red plate (right) and radio contours of the diffuse emission (after subtraction of discrete sources) overlaid onto the Rosat HRI X-ray image in the 0.1-2.4 keV band (left). We note that the X-ray image shows a double structure separated by less than $2'$. The radio diffuse emission is asymmetric, on the Northern side with respect to the X-ray brightness peaks. The estimated total flux density of the extended radio complex is 11.9 mJy. After subtraction of discrete sources (8.2 mJy), the halo total flux is 3.7 mJy.

Abell 1213 is a poor nearby Abell cluster at $z = 0.0469$, characterized by the presence of a dumbbell radio galaxy (the BCG) identified with a double radio source (4C29.41, B2 1113+29, Fanti et al. 1982). In the X-band it was detected by the Einstein (Jones & Forman 1999) and Rosat (Ledlow et al. 2003) satellites. The X-ray image shows a faint irregular emission. The estimated X-ray luminosity in the 0.1 - 2.4 keV band is 0.10×10^{44} erg/sec i.e. at least 10 times lower than that of any cluster presently known to host a radio halo (see Table 2). Optical and X-ray data suggest a non-relaxed structure.

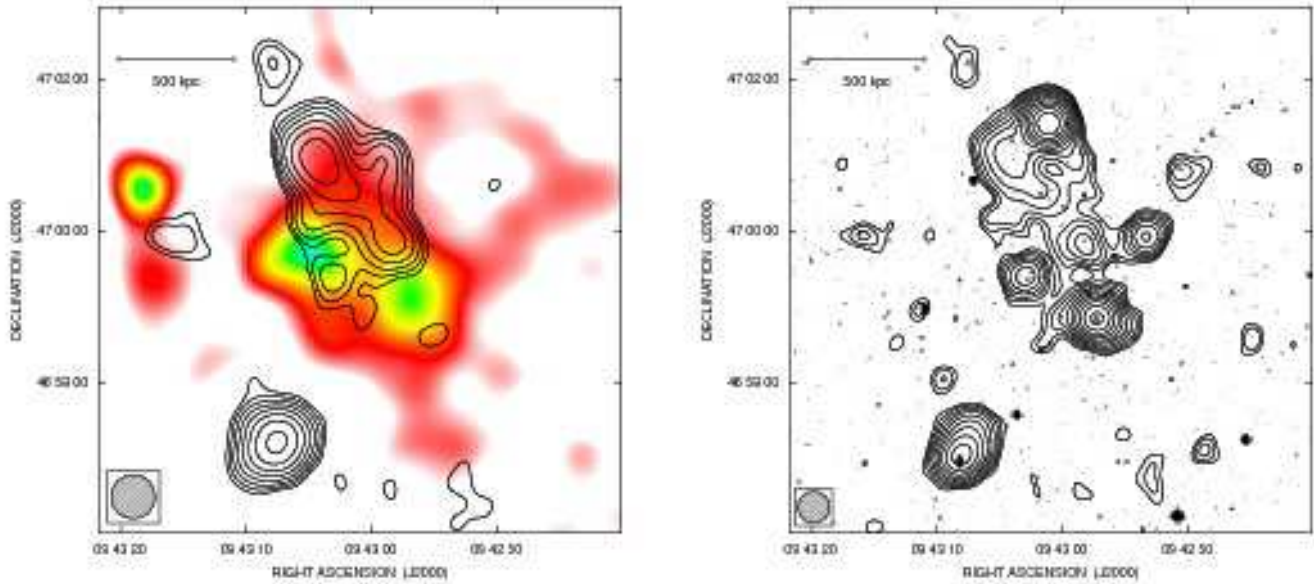


Fig. 4. Left: radio contours of A851 obtained with the VLA at 1.4 GHz combining data in C and D configuration, discrete sources in the cluster region have been subtracted. The HPBW is $35'' \times 35''$ and the noise level is 0.03 mJy/beam. The first contour level is drawn at 0.09 mJy/beam and the others are spaced by a factor $\sqrt{2}$. The contours of the radio intensity are overlaid onto the Rosat HRI X-ray image in the 0.1-2.4 keV band. The X-ray image has been smoothed with a Gaussian of $\sigma = 16''$. Right: radio contours as in the left figure but with no source subtraction. The HPBW is $25'' \times 25''$. The contours of the radio intensity are overlaid onto the optical image from the POSS2 red plate.

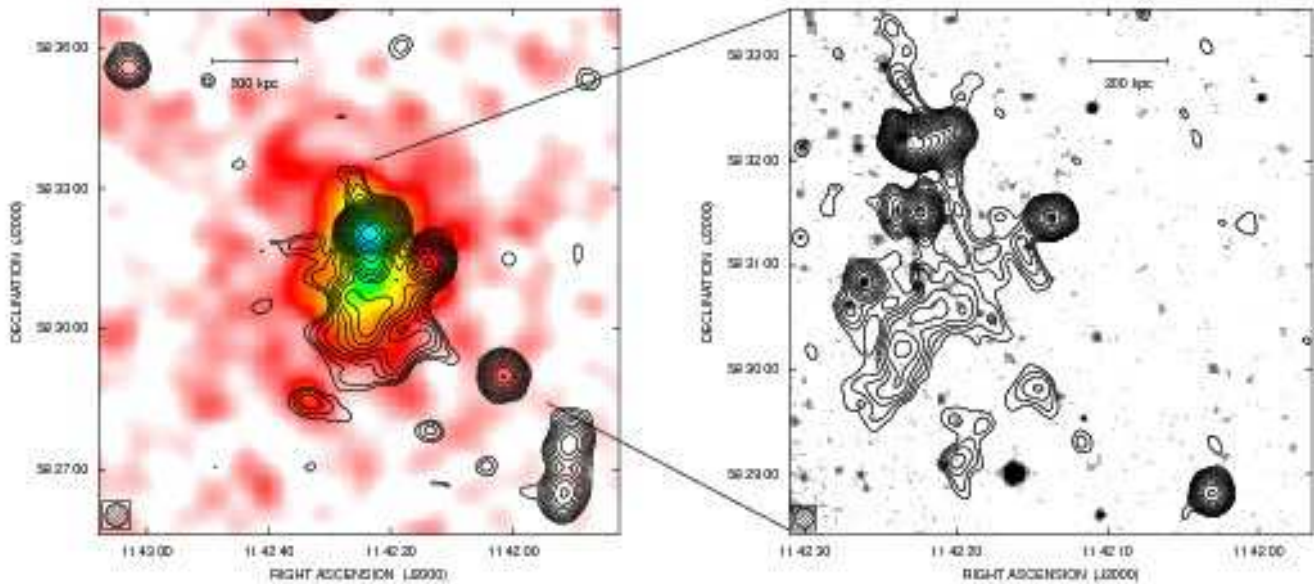


Fig. 6. Left: radio contours of the extended halo in A1351 obtained with the VLA at 1.4 GHz combining data in C+D configuration. The HPBW is $30'' \times 30''$ and the noise level is 0.09 mJy/beam. The first contour level is drawn at 0.25 mJy/beam and the others are spaced by a factor $\sqrt{2}$. The contours of the radio intensity are overlaid onto the Rosat HRI X-ray image in the 0.1-2.4 keV band. The X-ray image has been smoothed with a Gaussian of $\sigma = 16''$. Right: radio contours obtained with the VLA at 1.4 GHz in C configuration of A1351. The HPBW of the radio image is $11'' \times 11''$ and the noise level is 0.06 mJy/beam. The first contour level is drawn at 0.15 mJy/beam and the others are spaced by a factor $\sqrt{2}$. The contours of the radio intensity are overlaid onto the optical image from the POSS2 red plate.

The radio morphology of the BCG is peculiar being a small-size bright double similar to FR II radio galaxies. Moreover despite the small number of bright galaxies, at least

two other cluster members are identified as radio galaxies (A, B see Fanti et al. 1982 and Fig. 5). The FIRST survey (Becker et al. 1995) confirms Fanti et al. 1982 results, while the

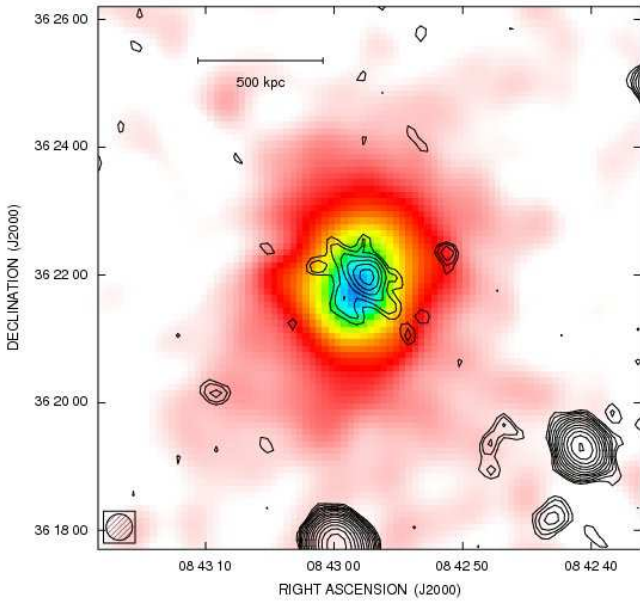


Fig. 3. Radio contours of A697 obtained with the VLA at 1.4 GHz in C configuration. The HPBW is $25'' \times 25''$ and the noise level is 0.04 mJy/beam. The first contour level is drawn at 0.1 mJy/beam and the others are spaced by a factor $\sqrt{2}$. The contours of the radio intensity are overlaid onto the Rosat HRI X-ray image in the 0.1–2.4 keV band. The X-ray image has been smoothed with a Gaussian of $\sigma = 16''$.

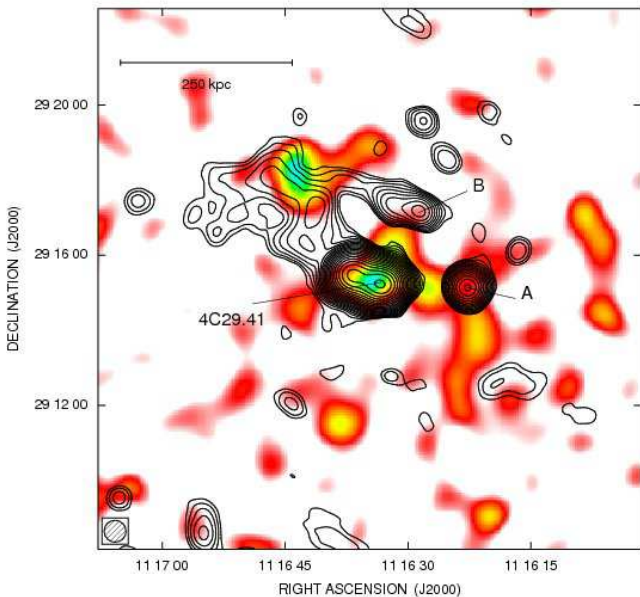


Fig. 5. Radio contours of A1213 obtained with the VLA at 1.4 GHz in C+C/D configuration. The HPBW is $35'' \times 35''$ and the noise level is 0.3 mJy/beam. The first contour level is drawn at 1 mJy/beam and the others are spaced by a factor $\sqrt{2}$. The contours of the radio intensity are overlaid onto the Rosat HRI X-ray image in the 0.1–2.4 keV band. The X-ray image has been smoothed with a Gaussian of $\sigma = 16''$. Cluster radio galaxies (the BCG 4C29.41, A, and B) are named according to the text.

NVSS detected a diffuse extended emission which cannot be due to the presence of the discrete sources found in the FIRST

image. The extended emission is off-center with respect to the BCG (NE direction). To better investigate this structure we obtained short VLA observations pointed on the cluster center in the C and C/D configuration. Our final image is presented in Fig. 5. The extended diffuse emission is easily visible. It is similar to small-size asymmetric radio halos found in other clusters as A2218 (Giovannini & Feretti 2000), and we classify it as a small-size radio halo. However the diffuse radio source shows a peculiar bright filament in the inner region with a sharp bend as a Z shaped structure. This filament is in direction of the BCG bright radio galaxy but it is not connected to it. The radio structure of 4C29.41 and the size of the diffuse component excludes a possible connection between the BCG and the diffuse structure due to a possible proper motion of the BCG.

A possible connection is also suggested by the radio morphology of the diffuse emission, with the source at north of the BCG, identified with a cluster elliptical galaxy (source B). This source shows a peak flux density in the FIRST images = 5.3 mJy/beam. It appears slightly resolved on the W side with respect to the galaxy position, i.e. on the opposite side to the extended diffuse emission. We cannot exclude that this source could be a head-tail radio galaxy, but the radio morphology and radio power rule out the possibility that all or most of the diffuse emission could be identified as an extended tailed structure. Therefore as discussed before we connect the extended source not to the activity of one or more cluster galaxies but to the physical properties of the whole cluster.

Abell 1351 is a rich massive cluster at $z = 0.3224$ with an elongated X-ray brightness distribution indicating a possible ongoing merger. It shows also an unusually high velocity dispersion, and the presence of a bright red gravitational arc offset from the cluster light center (Dahle et al. 2002).

Owen et al. 1999 reported the existence of a halo source in this cluster. We analyzed VLA archive data at 1.4 GHz in C and D configuration.

In Fig. 6 we show the cluster radio emission compared with optical and X-ray images. We produced a low resolution radio image to obtain a better signal to noise ratio for the halo source. On the left the contours of this image are overlaid onto the Rosat HRI X-ray image in the 0.1–2.4 keV band. On the right we show a zoom of radio contours at higher resolution overlaid onto an optical image. The presence of an extended diffuse radio halo source is easily visible even in the high resolution image which also shows 4 discrete sources. Two of these sources show an elongated head-tail like structure and are identified as possible cluster galaxies. We note that the radio-diffuse emission is centrally located but asymmetric with respect to the X-ray brightness peak.

In this cluster the subtraction of discrete sources was more problematic, because of the presence of two strong, extended tailed radio galaxies in the Northern region (see Fig. 6, right). For this reason we present in Fig. 6 left the image with no source subtraction. We checked the total flux density of the diffuse emission, obtained as discussed in Sect. 2, with the halo flux density obtained by integrating the central cluster region in the low resolution image, and subtracting the estimated flux density of discrete sources derived from a multi-component gaussian fit of discrete sources (JMFIT in AIPS). We found a good agreement between the two values.

Abell 1758 from the optical point of view, is a double cluster which is possibly in the process of merging into a single massive cluster. Both sub-clumps are concentrated around a bright early-

type galaxy. There is an apparent blue arc associated with the northwest mass clump (Dahle et al. 2002).

It was studied in detail in the X band by David & Kempner 2004. They confirm the double structure of this cluster: it consists of two hot X-ray luminous clusters: A1758N and A1758S. Moreover the two main clusters show a clear substructure: A1758N is in the late stage of a merger of two 7 keV subclusters, while A1758S is in the early stages of a merger of two 5 keV subclusters.

Giovannini et al. 2006 reported the detection of a radio halo in A1758N. Radio images show that the central emission is confused by unrelated discrete sources. After subtraction in the uv-plane we obtained a low resolution image of the extended emission. In Fig. 7 we present the radio contours of the extended halo source with the discrete sources subtracted. For a comparison between the radio and the X-ray cluster emission, the contours of the radio intensity are overlaid onto the Rosat HRI X-ray image in the 0.1-2.4 keV band of A1758N. The two peaks corresponding to the subclusters in the late merging phase are clearly visible. The radio image shows a complex structure similar to that of A754 (Kassim et al. 2001, Bacchi et al. 2003). In A1758N we identify a central diffuse emission (halo) permeating the central region where the two sub-clusters are merging, 0.8 Mpc in size (H in Fig. 7), and two brighter peripheral structures on the opposite side with respect to the cluster center, which resemble relic radio sources R in Fig. 7). A1758N would be one of the very few clusters with a central halo and two peripheral relics as in RXCJ1314.4-2515 (Feretti et al. 2005).

The detection of a radio-diffuse emission in A1758N and not in A1758S is consistent with the hotter temperature (7keV) of the Northern subclusters with respect to Southern subclusters (5 keV) and with the results of David & Kempner 2004: that A1758N is in a late stage of merger, while A1758S is in an early merger stage.

Abell 1995 is a rich massive cluster at $z = 0.3186$. The light distribution in this cluster is quite strongly elongated in the northeast-southwest direction, but the mass distribution is more circularly symmetric and concentrated. Moreover, Dahle et al. 2002 discussed the presence of several blue arcs. The X-ray morphology analyzed by Patel et al. 2000 appears very similar to the mass distribution.

Owen et al. 1999 reported the existence of a halo source in this cluster. We reduced VLA archive data in C and D configuration. An extended diffuse emission is clearly visible at the cluster center (Fig. 8 left). Two relatively bright point-like sources (Fig. 8 right) have been subtracted to estimate the halo parameters. The radio contours of the halo sources after subtraction of discrete sources are overlaid onto the Rosat HRI X-ray image in the 0.1-2.4 keV band. The original VLA image is overlaid onto the optical image from the POSS2 red plate.

Abell 2034 shows multiple signatures of an ongoing merger in a Chandra X-ray image, including a cold front and probable significant heating of the ICM (Kempner et al. 2003). In this region Kempner & Sarazin 2001 detected an extended radio emission North of the cluster center near to the position of the cold front. We analyzed archive VLA data at 1.4 GHz in C and D configuration to confirm and to image in detail the diffuse emission.

In Fig. 9 we show the cluster radio emission compared with the optical and X-ray images. On the left the contours of a low resolution image are overlaid onto the Rosat PSPC X-ray image in the 0.1-2.4 keV band. In the right panel we show a zoom

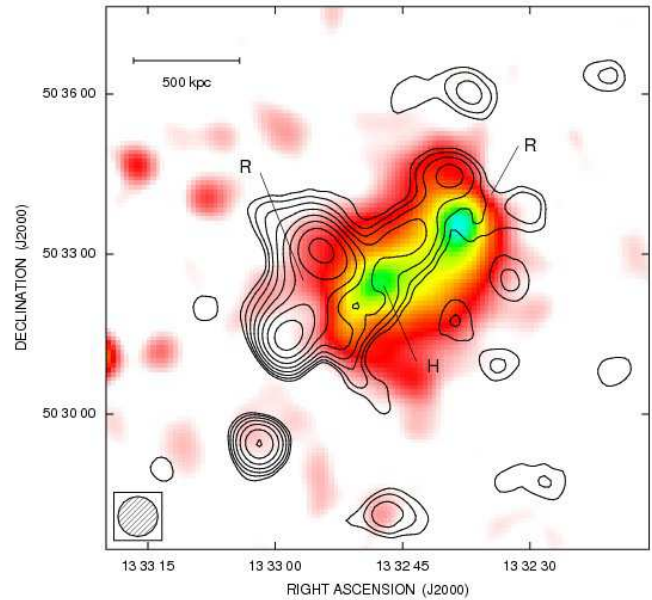


Fig. 7. Radio contours of A1758N obtained with the VLA at 1.4 GHz in configuration D, after subtraction of discrete sources. The HPBW is $45'' \times 45''$ and the noise level is 0.07 mJy/beam. The first contour level is drawn at 0.2 mJy/beam and the others are spaced by a factor $\sqrt{2}$. H and R show the halo and relic sources, see text. The contours of the radio intensity are overlaid onto the Rosat HRI X-ray image in the 0.1-2.4 keV band. The X-ray image has been smoothed with a Gaussian of $\sigma = 16''$.

of radio contours at higher resolution overlaid onto the optical image taken from the POSS2 red plate in the Optical Digitized Sky Survey. The diffuse radio emission is located at the cluster center, but with respect to other giant halos it appears elongated and irregular. The Northern region (pointed out by an arrow) of the diffuse source coincides with the tentative relic in the cold front region discussed by Kempner et al. 2003.

Abell 2294 is a rich massive cluster at $z = 0.178$ the temperature profile is consistent with an isothermal cluster at $T \sim 8$ keV (Rizza et al. 1998). Owen et al. 1999 reported the existence of a halo source in this cluster. We analyzed VLA data in the C and D configuration. In Fig. 10 we present the radio contours of A2294 after subtraction of discrete sources, overlaid onto the Rosat HRI X-ray image in the 0.1-2.4 keV band (left), and without source subtraction on the optical image from the POSS2 red plate (right). The diffuse radio emission, $3'$ in size, is in good agreement with the cluster X-Ray image.

Abell 3444 is a rich cluster at $z = 0.2533$. Matsumoto et al. 2001 were able to fit the ASCA spectra with a single-temperature thermal plasma model (5.7 keV). Lemonon (1999) and Matsumoto et al. 2001) defined A3444 as a possible cooling core cluster. Detailed optical studies are not available for this cluster.

We reduced VLA archive data at 1.4 GHz in A/B and C/D configuration. The low resolution image shows a very extended faint radio filament, located around a chain of discrete radio sources. Venturi et al. 2007 observed this cluster with the GMRT at 610 MHz and found that discrete radio sources have an optical counterpart and follow the inner elongation of the archive ASCA X-ray image. Moreover in GMRT images the dominant cluster

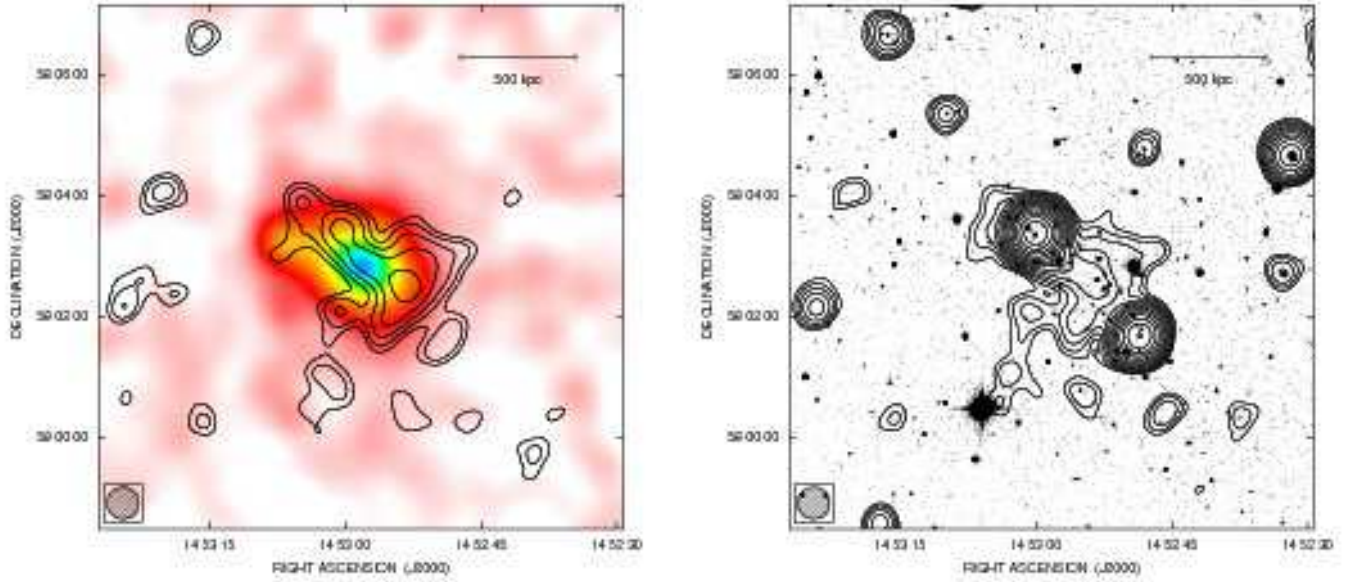


Fig. 8. Left: Radio contours of A1995 obtained with the VLA at 1.4 GHz in C+D configuration, after subtraction of discrete sources. The HPBW is $30'' \times 30''$ and the noise level is 0.05 mJy/beam. The first contour level is drawn at 0.1 mJy/beam and the others are spaced by a factor $\sqrt{2}$. The contours of the radio intensity are overlaid onto the Rosat HRI X-ray image in the 0.1-2.4 keV band. The X-ray image has been smoothed with a Gaussian of $\sigma = 16''$. Right: VLA radio image as in the left, but with no source subtraction. The radio contours are overlaid onto the optical image from the POSS2 red plate.

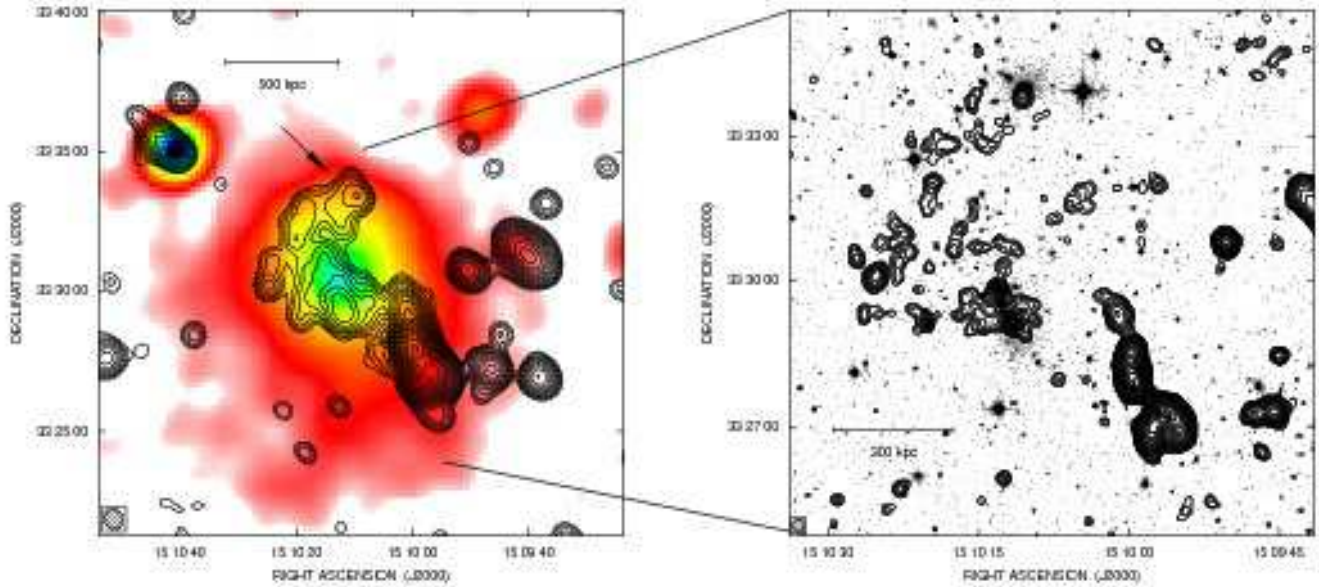


Fig. 9. Left: radio contours of the halo in A2034 obtained with the VLA at 1.4 GHz combining data in C+D configuration. The HPBW is $43.8'' \times 39.9''$ in PA 33° and the noise level is 0.04 mJy/beam. The first contour level is drawn at 0.1 mJy/beam and the others are spaced by a factor $\sqrt{2}$. The contours of the radio intensity are overlaid onto the Rosat PSPC X-ray image in the 0.1-2.4 keV band. The X-ray image has been smoothed with a Gaussian of $\sigma = 30''$. Right: radio contours obtained with the VLA at 1.4 GHz in C configuration of A2034. The HPBW of the radio image is $15.7'' \times 14.9''$ in PA -3° and the noise level is 0.016 mJy/beam. The first contour level is drawn at 0.04 mJy/beam and the others are spaced by a factor $\sqrt{2}$. The contours of the radio intensity are overlaid onto the optical image from the POSS2 red plate. An arrow points the cold front region (see text)

galaxy shows an extended radio emission, and a flux density of 10 mJy is present on a scale of $1.5'$ at 610 MHz.

Our high resolution image is presented on the top right and bottom panels of Fig. 11, where zooms of the radio contours in

different regions of the radio filament are overlaid onto an optical image. The radio emission of the central cD galaxy is clearly extended with a size of $45''$. The peak is 6.5 mJy/beam, and the total flux is 7.4 mJy. We classify this extended emission as a

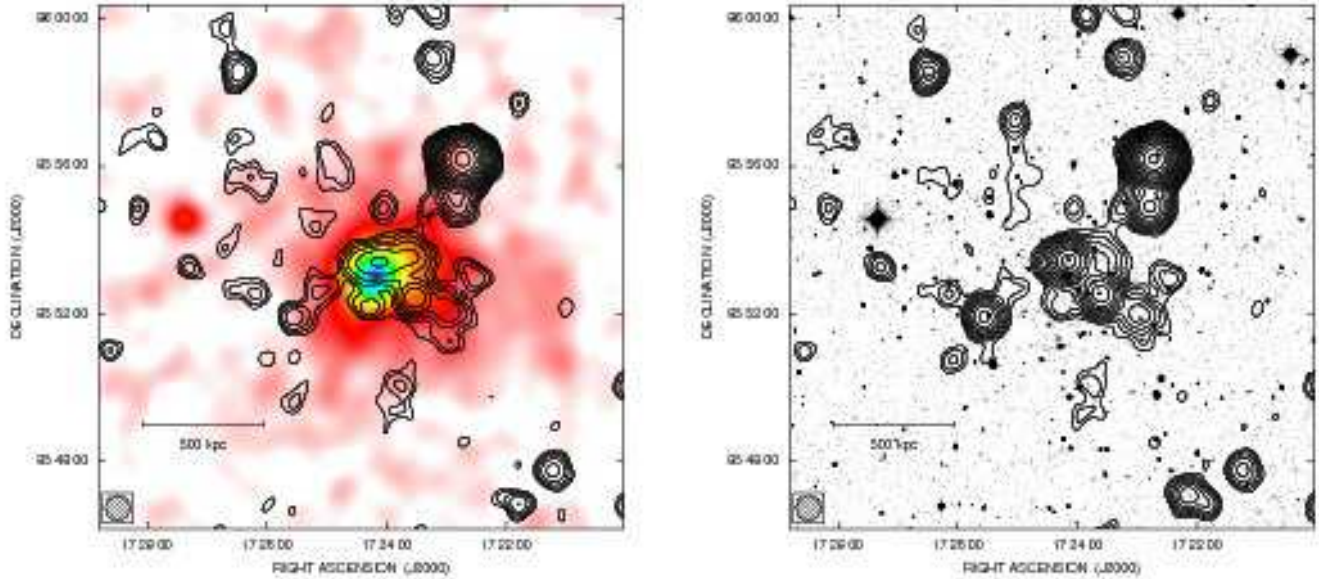


Fig. 10. Left: radio contours of A2294 obtained with the VLA at 1.4 GHz combining data in C and D configuration. Discrete sources in the cluster region have been subtracted. The HPBW is $35'' \times 35''$ and the noise level is 0.04 mJy/beam. The first contour level is drawn at 0.12 mJy/beam and the others are spaced by a factor $\sqrt{2}$. The contours of the radio intensity are overlaid onto the Rosat HRI X-ray image in the 0.1-2.4 keV band. The X-ray image has been smoothed with a Gaussian of $\sigma = 16''$. Right: as in the Left panel but without source subtraction. The contours of the radio intensity are overlaid onto the optical image from the POSS2 red plate.

faint 'mini-halo' diffuse source in agreement with the presence of a possible central cooling flow.

We subtracted in the uv-plane all the discrete sources embedded in the extended emission except the central cD galaxy, since it is clearly resolved in our images, so as to study a possible connection between it and the extended emission. This image is presented in Fig. 11 where the radio contours are overlaid onto the Rosat HRI X-ray image in the 0.1-2.4 keV band.

A clear filamentary structure $\sim 14'$ in size corresponding to 3.3 Mpc at the cluster distance is present, centered on the cD galaxy. However because of the large size and morphology we exclude a direct connection between the cD and this radio filament. We do not classify this extended and diffuse radio emission as a radio halo, but we suggest a connection with a possible filamentary structure as found by Bagchi et al. 2002, and Brown & Rudnick 2009. We note that the presence of a giant filamentary radio structure is not incompatible with a possible central cooling flow in A3444.

CL 1446+26 named also CL 1447+26 or ZwCl 1447.2+2619, has been discussed by Owen et al. 1999 who show a radio image overlaid onto an optical R-band image. We retrieved an archive VLA observation in C configuration and obtained a deeper image shown in Fig.12. The radio contours are overlaid onto the Rosat All Sky Survey X-ray image in the 0.1-2.4 keV band.

From a comparison with the FIRST and the Owen et al. 1999 image, it is clear that in this cluster two head-tail radio galaxies are present and appear blended in a strong unresolved source in our image at RA=14 49 30, DEC=+26 08 00 in the periphery of the diffuse emission. A third head tail radio galaxy is at RA=14 49 28 DEC=+26 08 20. Moreover a background source is north of the extended emission at RA=14 49 30 DEC=+26 09 10.

The X-Ray image shows an elongated emission with the presence of a secondary peak displaced by about 500 kpc up to

the NE. We interpret this substructure as evidence of a smaller group merging into the main cluster. The diffuse radio emission is in-between the two X-Ray peaks and for this reason it is more appropriate to identify it as a relic radio source.

4. Discussion

Next we present a few statistical considerations on the properties of radio halos combining radio halos taken from the literature with those presented above. We note that this is not a complete sample of radio halos therefore we cannot use it to analyze statistical properties such as the percentage of clusters with a radio halo or the radio halo luminosity function. However, the large number of halo sources collected here can be used to derive correlations and to obtain the observational properties of known radio halos.

In Tab. 2 we present all the known halos at $z < 0.4$ with a high quality pointed radio image, including literature data and sources presented for the first time in this work (see col. 8 for the references related to the radio data). Radio halos at larger redshift are rare. We will present results for higher redshift clusters in a forthcoming paper (but see Giovannini & Feretti 2000, and Bonafede et al. 2009b). We have a total of 33 sources; however, we note that in the case of CL1446+26 the diffuse source should be classified as a relic source and in A3444 the giant diffuse emission is likely a giant filament, and the extended emission around the cD galaxy a mini-halo. The final number of certain radio halos is therefore 31. The flux density of radio halos at 1.4 GHz and the estimated error are indicated in col. 4 and col. 5 of Tab. 2. The radio power at 1.4 GHz, and the radio Largest Linear Size (LLS) are given in col. 6 and col. 7. For each cluster in col. 8 we indicate the X-ray luminosity in the 0.1-2.4 keV band obtained from the references given in col. 10 and converted to the cosmology used in this paper. In the case of A1213

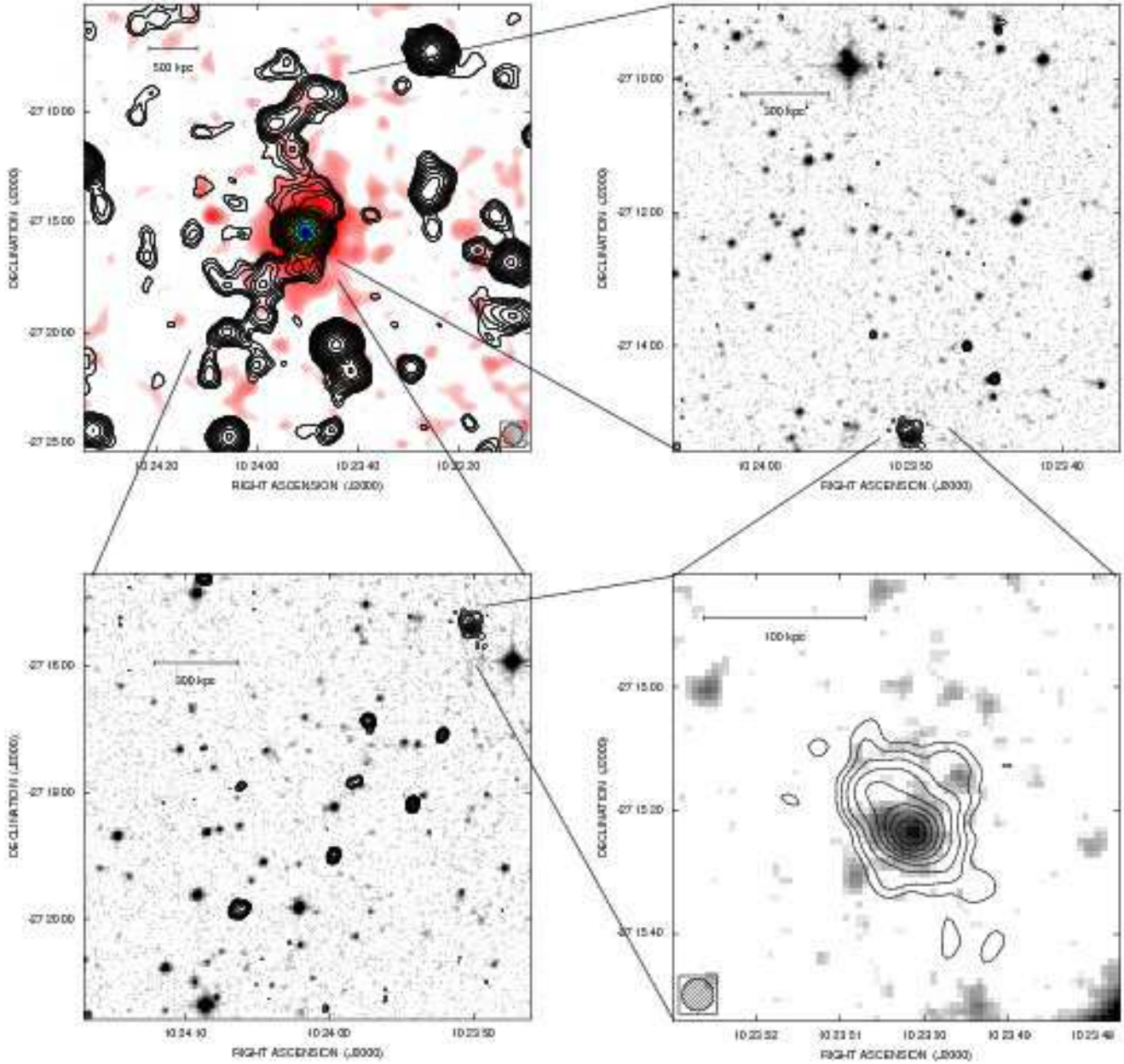


Fig. 11. Top, Left: radio contours of the diffuse filament located in A3444 obtained with the VLA at 1.4 GHz combining data in A/B and C/D configuration, after subtraction of discrete sources (but not the central cD). The HPBW is $55'' \times 55''$ and the noise level is 0.033 mJy/beam. The first contour level is drawn at 0.1 mJy/beam and the others are spaced by a factor $\sqrt{2}$. The contours of the radio intensity are overlaid onto the Rosat HRI X-ray image in the 0.1-2.4 keV band. The X-ray image has been smoothed with a Gaussian of $\sigma = 16''$. In this figure the restoring beam is in the bottom right corner. Top, Right: zoom to the north of the central cD galaxy of the VLA high resolution radio image. The HPBW is $5'' \times 5''$ and the noise level is 0.03 mJy/beam. The first contour level is drawn at 0.1 mJy/beam and the others are spaced by a factor $\sqrt{2}$. The contours of the radio intensity are overlaid onto the red optical image from the SERC/ESO surveys. Bottom, left: zoom to south of the central cD galaxy. Bottom, right: zoom of the central cD in A3444.

the X-ray emission in the 0.5-2 keV band (Ledlow et al. 2003) has been converted to the 0.1-2.4 keV band using Tab. 4 of Böhringer et al. 2004, while for CL1446+26 the bolometric X-ray emission (Wu et al. 1999) has been converted to the 0.1-2.4 keV band using Tab. 5 of Böhringer et al. 2004. In both cases we assumed an intra-cluster temperature value $T_X \approx 5$ keV.

4.1. Radio Morphology

Radio halos are generally extended sources located at the cluster center. The largest halo known so far is in A2163 (LLS = 2.28 Mpc), and many halos have a projected size larger than 1 Mpc. We note that the diffuse emission in A3444 is even more extended than A2163, but we consider its 3.3 Mpc structure as a giant filament very similar to the large scale structure seen in the filament of galaxies ZwCl 2341.1+0000 (Bagchi et al. 2002).

Table 2. Radio halos

Name	z	kpc''	S(1.4) mJy	ΔS mJy	log P(1.4) W/Hz	LLS Mpc	$L_x(10^{44})$ erg/sec	Ref. Radio	Ref. X-ray	notes
A209	0.2060	3.34	16.9	1.0	24.31	1.40	6.17	*	21	a relic could be present
A401	0.0737	1.38	17.0	1.0	23.34	0.52	6.52	1	15	elongated and irregular
A520	0.1990	3.25	34.4	1.5	24.58	1.11	8.30	2	16	
A521	0.2533	3.91	5.9	0.5	24.05	1.17	8.47	*	21	a relic is also present
A545	0.1540	2.64	23.0	1.0	24.16	0.89	5.55	1	21	
A665	0.1819	3.03	43.1	2.2	24.59	1.82	9.65	3	16	
A697	0.2820	4.23	7.8	1.0	24.28	0.65	10.40	*	16	from NVSS, see text
A754	0.0542	1.04	86.0	4.0	23.77	0.99	2.21	1	15	a relic is also present
A773	0.2170	3.48	12.7	1.3	24.23	1.25	7.95	2	16	
A851	0.4069	5.40	3.7	0.3	24.33	1.08	5.04	*	17	
A1213	0.0469	0.91	72.2	3.5	23.56	0.22	0.10	*	18	asymmetric
A1300	0.3072	4.49	20.0	2.0	24.78	1.3	13.73	4,5	21	a relic is also present
A1351	0.3224	4.64	39.6	3.5	25.12	0.84	5.47	*	17	
A1656	0.0231	0.46	530.0	50.0	23.80	0.83	3.99	6	15	a relic is also present
A1758	0.2790	4.20	16.7	0.8	24.60	1.51	7.09	*	19	total diffuse emission H+R central halo
			3.9	0.4	23.97	0.63		*		
A1914	0.1712	2.88	64.0	3.0	24.71	1.04	10.42	1	15	
A1995	0.3186	4.61	4.1	0.7	24.13	0.83	8.83	*	17	
A2034	0.1130	2.03	13.6	1.0	23.64	0.61	3.81	*	16	
A2163	0.2030	3.31	155.0	2.0	25.26	2.28	22.73	7	14	a relic is also present
A2218	0.1756	2.94	4.7	0.1	23.60	0.38	5.77	3	16	asymmetric
A2219	0.2256	3.58	81.0	4.0	25.08	1.72	12.19	1	16	
A2254	0.1780	2.98	33.7	1.8	24.47	0.92	4.55	2	16	irregular asymmetric shape
A2255	0.0806	1.50	56.0	3.0	23.94	0.90	2.64	8	16	a relic is also present
A2256	0.0581	1.11	103.4	1.1	23.91	0.81	3.75	9	16	a relic is also present
A2294	0.1780	2.98	5.8	0.5	23.71	0.54	3.90	*	16	
A2319	0.0557	1.07	153.0	8.0	24.04	1.02	8.46	10	15	spectral steepening
A2744	0.3080	4.50	57.1	2.9	25.24	1.89	12.86	2	21	a relic is also present
A3444	0.2533	3.91	14.6	1.0	24.45	3.3	13.42	*	21	Filament; see text
A3562	0.0490	0.95	20.0	2.0	23.04	0.28	1.57	11	15	spectral steepening
1E0657-56	0.2960	4.38	78.0	5.0	25.33	2.1	22.59	12	21	bullet cluster
RXCJ1314.4-2515	0.2439	3.81	20.3	0.8	24.55	1.83	10.75	13	21	Double relics are present
CL1446+26	0.3700	5.08	9.2	0.5	24.63	0.36	3.42	*	20	relic source
RXCJ2003.5-2323	0.3171	4.59	35.0	2.0	25.09	1.40	9.12	14	21	

Col. 1: Cluster Name; Col. 2: Redshift; Col. 3: Angular to linear conversion; Col. 4: Radio flux density at 1.4 GHz; Col. 5: Estimated flux density error;

Col. 6: Radio power at 1.4 GHz; Col. 7: Radio largest linear size; Col. 8: X-ray luminosity in the 0.1-2.4 keV band in 10^{44} units;

Col. 9: References for radio data:

* = This work; 1 = Bacchi et al. 2003; 2 = Govoni et al. 2001a; 3 = Giovannini & Feretti 2000; 4 = Venturi et al. 2009; 5 = Reid et al. 1999;

6 = Kim et al. 1990; 7 = Feretti et al. 2001; 8 = Govoni et al. 2005; 9 = Clarke & Enslin 2006;

10 = Feretti et al. 1997; 11 = Venturi et al. 2003; 12 = Liang et al. 2000; 13 = Feretti et al. 2005; 14 = Giacintucci et al. 2009.

Col. 10: References for X-ray data:

15 = Reiprich & Böhringer 2002; 16 = Ebeling et al. 1998; 17 = Böhringer et al. 2000; 18 = Ledlow et al. 2003; 19 = Ebeling et al. 1996; 20 = Wu et al. 1999; 21 = Böhringer et al. 2004.

Col. 11: Notes

Six radio halos have a size $\lesssim 0.5$ Mpc. However, the properties of the galaxy clusters and the absence of a strong centered radio galaxy indicate that these sources are very different from the mini-halo class of radio sources (see e.g. Govoni et al. 2009). We consider them as genuine halos of small size.

Most radio halos show a centrally located and regular radio morphology. In a few cases the radio source is elongated as e.g. in A209, A401, and A2034; however, we note that this shape is expected from merging clusters. X-Ray images of merging clusters can be elongated in the direction of the merger and because of the strong correlation between the X-ray and radio brightness distribution (Govoni et al. 2001b) we expect elongated radio halos. Probably the radio emission is still more complex and irregular with more substructures, as shown e.g. by the polarized filament in A2255 (Govoni et al. 2005), but the large HPBW necessary to detect the low radio brightness does not allow such a study.

A few radio halos are highly asymmetric, being located mostly on one side with respect to the cluster center. In A851,

A1351, A2218, and in the peculiar cluster A1213 we see these asymmetric sources. We interpret these structures as due to a highly asymmetric merger, but a more detailed comparison between radio and X-ray data is necessary.

We note that in 10 clusters with a radio halo we confirm the presence of one or two relic radio sources (see notes in Table 2). The high percentage ($\sim 30\%$) of clusters with both a relic and a halo source confirms the connection between these two classes of diffuse sources and cluster mergers. In this scenario the cluster turbulence arising from a cluster merger is the major mechanism responsible for the electron reacceleration in halo sources, moreover shock waves originated by major mergers are able to compress magnetic fields and reaccelerate electrons at the cluster periphery giving origin to relics.

4.2. Radio size and Power

In Fig. 13 we report the radio halo's largest size (LLS) versus the total radio power at 1.4 GHz. The LLS has been estimated in ra-

and DRAO data; A2319 observed by Feretti et al. 1997 with the WSRT; A754 visible in VLA images because of the elongated and irregular structure of the radio halo.

From this distribution we can derive an upper limit of about 2 Mpc for the halo size, probably related to the physical dimension of galaxy clusters, and the gas distribution. The lack of large halos at high redshift is apparent since we have only 1 halo at $z > 0.35$.

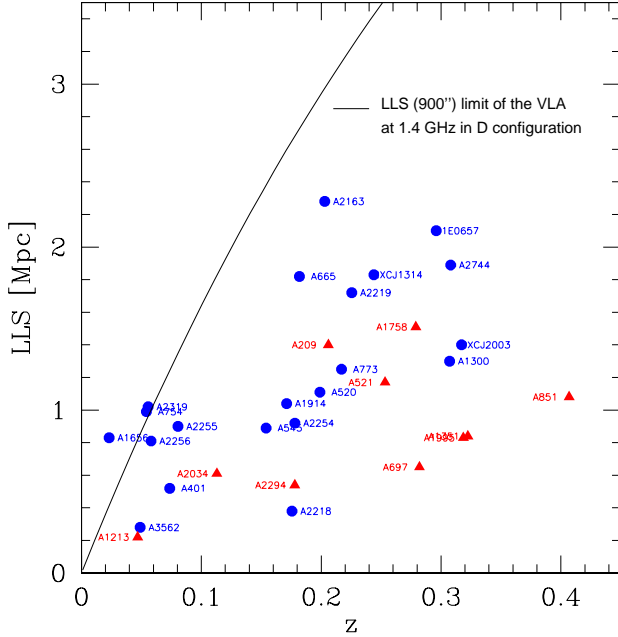


Fig. 15. Largest Linear size of radio halos in Mpc versus z . The upper line corresponds to a radio halo with a size = $15'$, the largest structure visible by VLA at 1.4 GHz in D configuration. Red triangles are new halos, blue dots are halos from literature data.

In Fig. 16 we show the trend of radio power with redshift. To discuss possible selection effects in the halo distribution shown in this figure we individuate the regions where it is possible to obtain radio data with present radio telescopes. The upper continuous line has been derived taking into account the largest angular size visible with the VLA at 1.4 GHz (as discussed in Fig. 15), and the correlation between size and radio power shown in Fig. 13. Halo sources in the region above the continuous line are not visible because their angular size is too large. The lower dotted line has been estimated assuming that most of the data are from relatively short VLA observations. We have considered a ~ 3 hours observing time. Therefore radio halos in the region below the dotted line are not present because of sensitivity limits. To derive this limit we have taken into account the brightness decrease because of the luminosity and angular size distance and the correlation between radio power and LLS. Clear selection effects are present. With available radio telescopes we can observe only radio halos in between the two lines, BUT we note that radio halos discussed here are distributed homogeneously in the allowed region. The present sample is not complete, but it is representative of radio halos that can be observed with present radio telescopes.

More sensitive observations with the VLA and the EVLA should allow us to detect possible fainter sources. We will need

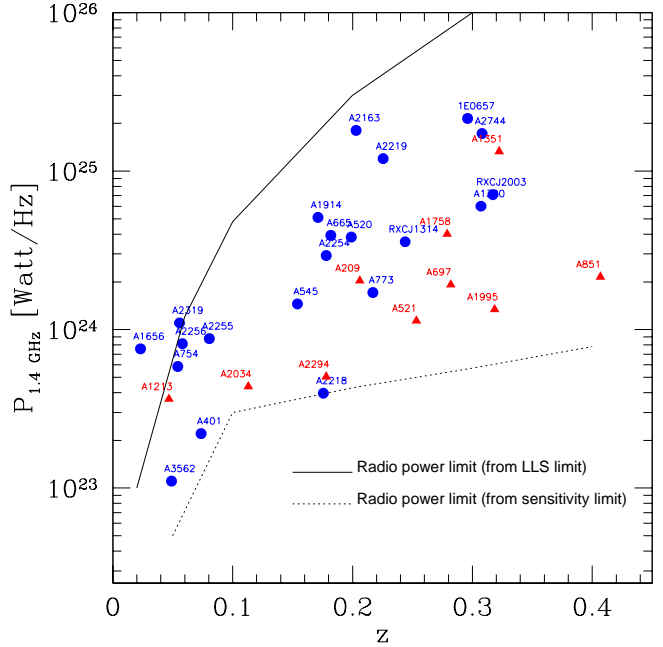


Fig. 16. Total radio power at 1.4 GHz versus z . The upper continuous line corresponds to a halo linear size corresponding to $15'$, the upper limit for VLA observations at 1.4 GHz. The lower dotted line is from an average sensitivity limit assuming a standard VLA observation with an integration time of ~ 3 hrs (see text). Red triangles are new halos, blue dots are halos from literature data.

to wait for the new generation of radio telescopes (LOFAR, SKA-pathfinders, SKA) to search for diffuse sources outside the present allowed region.

4.4. Spectral index

The integrated radio spectrum of halo sources is poorly known. These extended and diffuse sources always show a steep spectrum but only in a few cases the spectrum is derived with more than three flux density measurements at different frequencies. Moreover for most sources the highest available frequency is 1.4 GHz and the presence of a spectral steepening, crucial to discriminate between different reacceleration models, is difficult to determine.

Only four radio halos have a really well defined radio spectrum. The best studied integrated spectrum is still that for the Coma cluster where a clear evidence of a high frequency steepening is present (see Thierbach et al. 2003 for a detailed discussion). The steepest straight spectrum is shown by the radio halo in A1914 (Bacchi et al. 2003) where 9 different points show a straight spectrum with $\alpha = 1.88$. One more well studied halo is the one in A2256 (Brentjens 2008), and in 1E 0657 discussed in detail by Liang et al. 2000.

Feretti et al. 2004 investigated the existence of a possible correlation between the spectral index of radio halos and the cluster temperature. They found a marginal evidence that clusters at higher temperature tend to host halos with a flatter spectrum. To investigate this correlation we divided the radio halos with spectral information (Table 3) into three groups to enhance the statistical differences taking into account that the spectral index measures are highly inhomogeneous. For radio halos with

Table 3. Spectral Index of Radio halos

Name	α_1	α_2	Temperature keV	Reference
Straight	> 3 points			
A1914	$\alpha_{0.26}^{1.4} = 1.88$		7.9	1
A2256	$\alpha_{0.27}^{1.4} = 1.61$		6.6	7
1E 0657	$\alpha_{0.84}^{0.9} = 1.3$		10.6	10
Steepening	> 3 points			
A1656	$\alpha_{0.31}^{1.4} = 1.16$	$\alpha_{1.4}^{4.8} = 2.28$	8.4	11
Straight	3 points			
A521	$\alpha_{0.24}^{1.4} = 1.80$		5.9	*
RXC J2003	$\alpha_{0.2}^{1.4} = 1.3$		-	4
Steepening	3 points			
A754	$\alpha_{0.07}^{0.3} = 1.1$	$\alpha_{0.3}^{1.4} = 1.5$	9.5	1
A2163	$\alpha_{0.3}^{0.3} = 1.1$	$\alpha_{1.3}^{1.4} = 1.5$	13.3	5
A2319	$\alpha_{0.6}^{0.6} = 0.9$	$\alpha_{1.4}^{1.4} = 2.2$	8.8	8
A3562	$\alpha_{0.3}^{0.8} = 1.3$	$\alpha_{0.8}^{1.4} = 2.1$	5.2	9
	2 points			
A545	$\alpha_{1.3}^{1.6} > 1.4$		5.5	1
A665	$\alpha_{0.3}^{1.4} = 1.04$		9.0	3
A697	$\alpha_{0.3}^{1.4} = 1.2$		10.2	*
A1300	$\alpha_{1.3}^{1.4} = 1.8$		9.2	4
A2218	$\alpha_{3.0}^{0.6} = 1.6$		7.1	3
A2219	$\alpha_{0.3}^{1.4} = 0.9$		12.4	2
A2255	$\alpha_{0.3}^{1.4} = 1.7$		6.9	6
A2744	$\alpha_{0.3}^{1.4} = 1.0$		10.1	2

Notes: Temperature is the average cluster Temperature in keV from literature data;

References to spectral index information:

* = This work; 1 = Bacchi et al. 2003; 2 = Orru' et al. 2007;

3 = Giovannini & Feretti 2000; 4 = Venturi et al. 2009;

5 = Feretti et al. 2001; 6 = Govoni et al. 2005;

7 = Brentjens 2008; 8 = Feretti et al. 1997;

9 = Venturi et al. 2003; 10 = Liang et al. 2000; 11 = Thierbach et al. 2003.

a steepening spectrum we considered the average value in the range between 0.3 and 1.4 GHz. Because of the short frequency range we did not include A545. We obtained the following result:

- radio halos in clusters with an average temperature less than 8 keV, show an average spectral index of 1.7;
- radio halos in clusters with a temperature in the range from 8 to 10 keV, show an average spectral index of 1.4;
- halos in clusters with a temperature greater than 10 keV show an average spectral index of 1.1.

Despite the uncertainties due to highly inhomogeneous spectral index measures, this result indicates that hotter cluster tend to host halos with flatter spectra. This may be understood in the framework of acceleration models, since the hottest clusters are more massive and may host more recent violent mergers able to reaccelerate relativistic particles giving origin to halos with a flatter radio spectrum.

Note that in Table 3 we do not report uncertainties on the spectral index value, because: i) in well known radio spectra (more than 3 points) the spectral index is well determined, with an uncertainty due to the best fit procedure (usually of the order of 0.01); ii) in other radio spectra with only 2 or 3 points the formal error on the spectral index value is formally of the order of 0.1, *but* the largest uncertainty is the possible presence of a change in the radio spectrum curvature (e.g. steepening) which cannot be seen with only 2 - 3 points. We think that this uncertainty is minimized by our statistical approach to separate radio halos with spectral index information in 3 groups.

4.5. Radio X-ray correlation

In Fig. 17 we present the relation between the halo radio power at 1.4 GHz and the X-ray Luminosity. The distribution of present data is in agreement with previous results of this well known relation (see e.g. Bacchi et al. 2003, Feretti 2005b), but we have now a larger sample with a larger range in X-ray Luminosity and radio power. We note that this correlation is not generally applicable to all clusters but is present only between radio halos and parent galaxy clusters: relaxed, cooling clusters have not to be considered for this correlation.

The only cluster outside the correlation is Abell 1213 whose peculiarity has been already discussed in Sects. 3 and 4.2. It is the cluster in our sample with the lowest X-ray Luminosity (0.10×10^{44} erg/sec in the 0.1 - 2.4 keV band (see Table 2). The diffuse radio emission is the smallest (220 kpc) source discussed here, but because of its low redshift it is well resolved in NVSS images and confirmed by pointed observations obtained by us. This cluster could belong to a poorly known class of objects where a diffuse radio emission is present despite the very low X-ray emission.

5. Conclusion

We have presented data on all the radio halos in clusters at $z < 0.4$ observed up to now. Adding new results (from proprietary and archive VLA data) to published data, we collected an homogeneous sample of 31 radio halos. Data at 1.4 GHz are available for all sources. From a study of this large sample we have concluded that:

- Feretti, L., & Giovannini, G. 2008, A Pan-Chromatic View of Clusters of Galaxies and the Large-Scale structure, edited by M. Plionis, O. Lopez-Cruz and D. Hughes. Lecture Notes in Physics Vol. 740.474, p.143
- Ferrari, C., Arnaud, M., Ettori, S., et al., 2006, A&A, 446, 417
- Ferrari, C., Govoni, F., Schindler, S., Bykov, A.M., & Rephaeli, Y. 2008, Space Science Reviews, 134, 93
- Giacintucci, S., Venturi, T., Bardelli, S., et al., 2006, New Astronomy, 11, 437
- Giacintucci, S., Venturi, T., Macario, G., et al. 2008, A&A, 486, 347
- Giacintucci, S., Venturi, T., G. Brunetti, et al. 2009, A&A, in press; arXiv:0905.3479
- Giovannini, G., Tordi, M., Feretti, L. 1999, NewA, 4, 141
- Giovannini, G., & Feretti, L. 2000, New Astronomy, 5, 335
- Giovannini, G., & Feretti, L. 2004, Journal of Korean Astronomical Society, 37, 323
- Giovannini, G., Feretti, L., Govoni, F., et al., 2006, Astronomische Nachrichten, 327, 563
- Girardi, M., Boschin, W., & Barrena, R. 2006, A&A, 455, 45
- Govoni, F., Feretti, L., Giovannini, et al., 2001a, A&A, 376, 803
- Govoni, F., Ensslin, T.A., Feretti, L., Giovannini, et al., 2001b, A&A, 369, 441
- Govoni, F., & Feretti, L. 2004, International Journal of Modern Physics D, 13, 1549
- Govoni, F., Markevitch, M., Vikhlinin, A., et al., 2004, ApJ, 605, 695
- Govoni, F., Murgia, M., Feretti, L., et al., 2005, A&A, 430, L5
- Govoni, F., Murgia, M., Markevitch, M. et al., 2009, A&A, 499, 371
- Jones, C., & Forman, W. 1999, ApJ, 511, 65
- Kassim, N. E., Clarke, T. E., Enßlin, T. A., et al., 2001, ApJ, 559, 785
- Kempner, J. C., & Sarazin, C. L. 2001, ApJ, 548, 639
- Kempner, J. C., Sarazin, C. L., & Markevitch, M. 2003, ApJ, 593, 291
- Kim, K.-T., Kronberg, P. P., Dewdney, P. E., Landecker, T. L. 1990, ApJ, 355, 29
- Liang, H., Hunstead, R. W., Birkinshaw, M., & Andreani, P. 2000, ApJ, 544, 686
- Ledlow, M. J., Voges, W., Owen, F. N., & Burns, J. O. 2003, AJ, 126, 2740
- Lemonon, L. 1999, Ph.D. Thesis Universite' de Paris XI
- Matsumoto, H., Pierre, M., Tsuru, T. G., & Davis, D. S. 2001, A&A, 374, 28
- Mercurio, A., Girardi, M., Boschin, W., et al., 2003, A&A, 397, 431
- Murgia, M., Govoni, F., Markevitch, M., et al., 2009, A&A, 499, 679
- Orru', E., Murgia, M., Feretti, L., Govoni, F., Brunetti, G., Giovannini, G., et al., 2007, A&A, 467, 943
- Owen, F., Morrison, G., & Voges, W. 1999, Diffuse Thermal and Relativistic Plasma in Galaxy Clusters, 9
- Patel, S. K., Marshall, J., Carlstrom, J.E., et al. 2000, ApJ, 541, 37
- Paulin-Henriksson, S., Antonuccio-Delogo, V., Haines, C.P., et al., 2007, A&A, 467, 427
- Petrosian, V. 2001, ApJ, 557, 560
- Reid, A. D., Hunstead, R. W., Lemonon, L., & Pierre, M. M. 1999, MNRAS, 302, 571
- Reiprich, T. H., Böhringer, H. 2002, ApJ, 567, 716
- Rizza, E., Burns, J. O., Ledlow, et al., 1998, MNRAS, 301, 328
- Sato, T., & Martin, C. L. 2006, ApJ, 647, 946
- Thierbach, M., Klein, U., & Wielebinski, R. 2003, A&A, 397, 53
- Venturi, T., Bardelli, S., Dallacasa, D., et al. 2003, A&A, 402, 913
- Venturi, T., Giacintucci, S., Brunetti, G., et al. 2007, A&A, 463, 937
- Venturi, T., Giacintucci, S., Dallacasa, D., et al. 2008, A&A, 484, 327
- Venturi, T., Giacintucci, S., Cassano, R., et al. 2009, "The Low Frequency Radio Universe", ASP Conference Series, arXiv:0903.2934
- Wu, X.-P., Xue, Y.-J., & Fang, L.-Z. 1999, ApJ, 524, 22